Journal of Catalysis 429 (2024) 115196

Contents lists available at ScienceDirect

Journal of Catalysis

journal homepage: www.elsevier.com/locate/jcat

Atomically dispersed zeolite-supported rhodium complex: Selective and stable catalyst for acetylene semi-hydrogenation

Yuxin Zhao [a,b], Özge D. Bozkurt [a,b], Samira F. Kurtoğlu-Öztulum [a,b], Melisa Su Yordanli [c], Adam S. Hoffman [d], Jiyun Hong [d], Jorge E. Perez-Aguilar [d], Aylin Saltuk [c], Deniz Akgül [c], Oktay Demircan [c], Tülay A. Ateşin [e], Viktorya Aviyente [c], Bruce C. Gates [f], Simon R. Bare [d], Alper Uzun [a,b,g,*]

[a] Department of Chemical and Biological Engineering, Koç University, Rumelifeneri Yolu, Sarıyer 34450, Istanbul, Turkey
[b] Koç University TÜPRAŞ Energy Center (KUTEM), Koç University, Rumelifeneri Yolu, Sarıyer 34450, Istanbul, Turkey
[c] Department of Chemistry, Faculty of Arts and Sciences, Bogazici University, Bebek 34342, Istanbul, Turkey
[d] SSRL, SLAC National Accelerator Laboratory, Menlo Park, CA 94025, United States
[e] Department of Chemistry, The University of Texas Rio Grande Valley, Edinburg, TX, 78539-2999, United States
[f] Department of Chemical Engineering, University of California, Davis, CA 95616, United States
[g] Koç University Surface Science and Technology Center (KUYTAM), Koç University, Rumelifeneri Yolu, Sariyer, 34450 Istanbul, Turkey

ARTICLE INFO

Keywords:
Supported rhodium complexes
Zeolite
Acetylene semi-hydrogenation
Electronic structure effect
Density functional theory

ABSTRACT

Supported rhodium catalysts are known to be unselective for semi-hydrogenation reactions. Here, by tuning the electronic structure of supported mononuclear rhodium sites determined by the metal nuclearity and the electron-donor properties of the support, we report that atomically dispersed HY zeolite-supported rhodium with reactive acetylene ligands affords a stable ethylene selectivity > 90 % for acetylene semi-hydrogenation at 373 K and atmospheric pressure, even when ethylene is present in a large excess over acetylene. Infrared and X-ray absorption spectra and measurements of rates of the catalytic reaction complemented with calculations at the level of density functional theory show how the catalyst performance depends on the electronic structure of the rhodium, influenced by the support as a ligand that is a weak electron donor.

1. Introduction

When they are dispersed atomically on supports, noble metals offer yet undiscovered catalytic properties and prospects for applications [1–3]. Examples of such catalysts are gold (for low-temperature CO oxidation [4], acetylene hydrochlorination [5], and the water–gas shift reaction [6,7]) and other noble metals for alkene hydroformylation [8–10], selective hydrogenation [11–13], and methane partial oxidation [14–15]. As in molecular homogeneous catalysis, the electronic structures and catalytic properties of the metal centers depend sensitively on the metal nuclearity and the ligands on the metal, which include the support [16].

Molecular rhodium complexes offer a wide range of catalytic properties, finding technological applications for alkene hydrogenation [17] and hydroformylation [18], and methanol carbonylation [19]. To achieve the technological advantages offered by solid catalysts—ease of separation from products and lack of corrosion—researchers have investigated many rhodium complexes anchored to supports [20–23]. Now, we show how to tune the catalytic properties of atomically dispersed rhodium on a support to optimize it for a technologically important reaction, selective acetylene semi-hydrogenation [24–27]—a reaction for which rhodium has heretofore not been reported to provide high selectivity or stability in operation [28,29].

2. Experimental and computational methods

2.1. Materials and methods

Standard air-exclusion techniques were used in the synthesis and treatment of all the catalyst samples involved in this work. Zeolites and metal oxides, used as supports, were purchased from Zeolyst International and Merck, respectively, at the highest available purities. Before

* Corresponding author at: Department of Chemical and Biological Engineering, Koç University, Rumelifeneri Yolu, Sarıyer 34450, Istanbul, Turkey.
E-mail address: auzun@ku.edu.tr (A. Uzun).

https://doi.org/10.1016/j.jcat.2023.115196
Received 14 September 2023; Received in revised form 30 October 2023; Accepted 1 November 2023
Available online 4 November 2023

catalyst synthesis, the supports were calcined in flowing oxygen as the temperature was ramped to a target value at a rate of 3 K/min and held at that temperature for 4 h, followed by evacuation at the target temperature for 12 h. The target calcination temperatures were 973 K for MgO and ZrO_2; 793 K for SiO_2, 773 K for HY zeolites, Beta zeolites, Fe_2O_3; and γ-Al_2O_3; and 673 K for TiO_2 and ZnO. After calcination, the supports were transferred to an argon-filled MBraun glovebox (oxygen concentration < 0.5 ppm, water concentration < 0.5 ppm). To synthesize supported $Rh(CO)_2$ complexes with rhodium loadings of 1.0 wt%, 25 mg of $Rh(CO)_2$(acac) precursor (Merck, 98 %; acac is acetylacetonato ($[C_5H_7O_2]^-$)) was mixed with 975 mg of each of the calcined supports in *n*-pentane that had been purified by column chromatography in an MBraun SBS solvent purification system. The resultant slurry was stirred in a sealed flask for 24 h, followed by evacuation for 12 h to remove the *n*-pentane, leaving all the rhodium on the support. Each sample after evacuation was transferred to the glovebox. A similar procedure was followed to synthesize an HY zeolite-supported rhodium complex incorporating ethylene ligands, with the precursor being Rh $(C_2H_4)_2$(acac).

To synthesize supported rhodium clusters with various nuclearities, the HY zeolite-supported rhodium complex, $Rh(CO)_2$/HY zeolite, was treated in flowing hydrogen under various conditions. The $Rh(CO)_2$/HY zeolite sample was heated in flowing helium as the temperature was ramped at a rate of 3 K/min to a target temperature, whereupon the flowing gas was switched from helium to 50 vol% hydrogen (balanced with helium) and held under these reduction conditions at 373 K for 5, 20, or 60 min; at 473 K for 60 min; or at 573 K for 60 min, to yield the samples designated as Rh/HY zeolite-0.5 nm, Rh/HY zeolite-0.8 nm, Rh/HY zeolite-1.0 nm, Rh/HY zeolite-1.2 nm, and Rh/HY zeolite-1.3 nm, respectively, with the sample names reflecting the characterization data mentioned below. After the reduction of each sample, the gas stream was switched back to helium and the sample cooled to room temperature. The reduced samples were stored in the glovebox.

2.2. Fourier transform infrared (FTIR) spectroscopy

IR spectra of the solid samples were measured in transmission mode with a spectral resolution of 2 cm^{-1} using a Bruker Vertex 80v FTIR spectrometer equipped with a vacuum sample chamber. Samples were handled at room temperature, under vacuum (pressure < 2 hPa), or in the glovebox to exclude air and moisture. Before the spectroscopy experiments, each sample in the glovebox was pressed between two KBr windows in a holder and immediately transferred to the sample chamber of the spectrometer. The chamber was evacuated within seconds after insertion of the sample. Each reported spectrum is an average of 128 scans, and 128 background spectra of the KBr windows were collected before each measurement.

2.3. X-ray absorption spectroscopy (XAS)

XAS experiments were performed at beam line 4–1 of the Stanford Synchrotron Radiation Lightsource (SSRL), with the storage ring energy and current being 3 GeV and 500 mA, respectively. The double-crystal Si (220) monochromator was detuned by 25 % at the Rh K-edge to minimize the effects of harmonics. Each supported rhodium complex (50–80 mg containing 1.0 wt% rhodium) was pressed into a wafer and mounted in a sealed *in-situ* XAS cell [30] in an argon-filled glovebox at the synchrotron. For energy calibration, the absorption of a rhodium foil mounted downbeam of the sample was measured as measurements of the samples were made. Extended X-ray absorption fine structure (EXAFS) spectra were collected from 200 eV below the Rh K-edge (23220.0 eV) to values of the wave vector $k = 15.3$ $Å^{-1}$ in 15 min, with four scans collected and averaged for good signal-to-noise ratios.

Data analysis was performed using ATHENA and ARTEMIS [31]. ATHENA was used for data alignment, edge calibration (the edge energy of the reference channel was calibrated in each scan to the known Rh K-edge), and Linear Combination Fitting (LCF) analysis. ARTEMIS was used for the XAS modeling. Reference files used in the data analysis were calculated using the code FEFF7.0 [32].

The crystal structures of $[Rh(I)(CO)_2(acac)]$ [33] and $[Rh(I)(C_2H_4)_2(acac)]$ [34] were used to calculate the phase shifts and backscattering amplitudes representing the Rh–C_{CO}, Rh–O_{CO}, Rh–C, and Rh–O_s scattering paths (s represents short), as the structure of the supported mononuclear rhodium species was expected to be similar to those of these precursors [35]. The Rh–C_{CO} and multiple scattering paths of the Rh–O_{CO} of the carbonyl group were fitted together to separate out the carbon and oxygen first shells. The phase shifts and backscattering amplitudes representing Rh–Al, Rh–Si, Rh–Zn, and Rh–Mg scattering paths were calculated from the structural parameters characterizing Rh–Al, Rh–Si, Rh–Zn, and Rh–Mg alloys, respectively [36]. Iterative fitting was carried out for various plausible structural models until the best agreement was attained between the calculated k^1-, k^2-, and k^3-weighted EXAFS data and the postulated model. The fitting ranges in both *k*-space and *R*-space (where *R* is the distance from the absorbing rhodium atom) in the analysis of the data characterizing the as-prepared sample were determined by the data quality. The range in *k* was in general (3.5 ± 0.5)–(12.8 ± 0.8 $Å^{-1}$), and the range in *R* was (1.0 ± 0.5)–(3.5 ± 0.5) Å for each supported mononuclear rhodium complex. These values were used with the Nyquist theorem [37] to estimate the justified number of fitting parameters, which was never exceeded in the reported best fits.

In analysis of data characterizing supported rhodium clusters, the crystal structure of fcc-rhodium (rhodium foil) was used to calculate the phase shifts and backscattering amplitudes representing the Rh–Rh and Rh–Rh_2 scattering paths (i.e., the nearest-neighbor, at approximately 2.7 Å, and the second-nearest-neighbor, at approximately 3.8 Å, scattering paths), respectively. Fitting was carried out considering k^1-, k^2-, and k^3-weighting. The fitting ranges in both *k* space and *R* space in the analysis of the data characterizing the as-prepared sample were determined by the data quality. The range in *k* was in general 4.0–14.0 $Å^{-1}$, and the range in *R* was (1.0 ± 0.1)–(3.9 ± 0.1) Å for each catalyst containing supported rhodium clusters.

2.4. Aberration-corrected scanning transmission electron microscopy (AC-STEM)

AC-STEM images were obtained with a Hitachi HF5000 Cs-corrected cold FEG scanning transmission electron microscope operating at 200 kV. In an argon-filled glovebox near the instrument, each sample was prepared on a Ted Pella lacey carbon-coated 300 mesh copper grid. The grid was transferred to the microscope in a sample holder filled with argon. A 30-μm STEM condenser aperture was used, and dark field images were obtained at a magnification of 800 k×. Nanocluster diameters were determined with Nano Measurer 1.2 software.

2.5. Thermogravimetric analysis (TGA)

TGA data characterizing the fresh and used Rh/HY zeolite-1.3 nm catalysts were obtained with a TA Instruments TGA Q500 instrument. The temperature of each sample (approximately 10 mg, in a platinum holder) was raised to 398 K at a rate of 20 K/min in a mixture of flowing dry air (40 mL/min) and nitrogen (60 mL/min) and then maintained at 398 K for 2 h to remove any adsorbed moisture. Then the temperature was increased to 1023 K at a rate of 5 K/min with the same flowing gas, and the mass of the sample was recorded during the process.

2.6. Density functional theory (DFT) calculations

Density functional theory calculations were done with the Gaussian 16 series of programs [38]. The PBE functional [39,40], along with the standard 6–31 + G(d,p) basis set, as well as the LANL2DZ basis set of Hay and Wadt for rhodium were used to perform full geometrical

optimizations [41,42]. Energies stated in the text are the Gibbs free energies calculated at 373 K and 1 atm and obtained by frequency calculations at the above-stated level of theory. The charge analysis was carried out using Charge Model 5 (CM5), as reported previously [43–45].

2.7. Catalyst performance measurements

Catalytic activity testing was performed with each sample in a 0.5-inch-diameter quartz tubular once-through flow reactor. The reaction temperature was controlled with a PC-operated Thermcraft three-zone resistance heating furnace (Model XST-3-0-18-3V). Gas flow rates were controlled with calibrated Alicat MC mass flow controllers. If not otherwise specified, the reactant feed gases (hydrogen, acetylene, ethylene, and helium) flowed through a bed containing 100 mg of catalyst particles at atmospheric pressure and a target temperature. When the supported catalysts initially incorporated mononuclear rhodium carbonyl complexes, they were treated in flowing acetylene as the reactor was heated from room temperature to 373 K at a rate of 3 K min^{-1} and held at 373 K for 60 min to convert the almost inactive rhodium carbonyl complex to a rhodium complex incorporating acetylene ligands. Subsequently, the catalysts were tested at atmospheric pressure and 373 K with a feed of acetylene (Linde, 99.9 vol%) and hydrogen (Linde, 99.99 vol%) in a 1:1 M ratio with a total flow rate of 10 mL(NTP)/min. The product stream was analyzed with an online gas chromatograph (Agilent GC 7890A) with a GS-Alumina column (50 m × 530 μm) and a hydrogen flame ionization detector.

The acetylene conversions were in the differential range, <2 %. Reaction rates are reported per rhodium atom, that is, as turnover frequencies (TOF), assuming that all the rhodium atoms were accessible for reaction. Thus, TOFs were calculated according to the fraction of exposed rhodium atoms for catalysts with various nuclearities (when rhodium clusters were less than 1 nm in diameter, the rhodium dispersion was considered to be 100 %; when rhodium clusters had diameters greater than 1 nm, the rhodium dispersion was approximated by $1/D_{cluster}$, where $D_{cluster}$ is the average cluster diameter in nm, estimated by assuming an fcc structure and using the corresponding first-shell Rh−Rh coordination number as determined by EXAFS analysis (details below). Repeated measurements were made with most of the samples to check for reproducibility. Three measurements of rate were typically measured for a sample, and the data lead to the conclusion the reaction rates were reproducible within ±5 %, consistent with the expected experimental errors.

3. Results

3.1. Synthesis and characterization of supported rhodium carbonyl complexes

The mononuclear supported rhodium carbonyl complexes were synthesized by the reaction of $Rh(CO)_2(acac)$ with supports chosen to have various electron-donor properties [36,46]. The supports included highly dealuminated zeolites HY and Beta, SiO_2, γ-Al_2O_3, ZrO_2, Fe_2O_3, TiO_2, ZnO, and MgO. As shown in Figures S1–S9 in the Supporting Information, the bands in the 1300–1700 cm^{-1} region of the IR spectra (Table S1) match those of the structure obtained by adsorption of acetylacetonate (Hacac) on the support, indicating the formation of Hacac by the reaction of the acac ligand in the precursor with support hydroxyl groups [47]. The results demonstrate that chemisorption involves the removal of acac ligands from the precursor $Rh(CO)_2(acac)$.

IR spectra of the initially prepared supported rhodium complexes (Figures S1-S9) include ν_{CO} bands similar to those of the precursor $Rh(CO)_2(acac)$, including ν_{COsym} and ν_{COasym} stretches at 2065 and 2007 cm^{-1} indicating the presence of rhodium *gem*-dicarbonyls (weak bands at 2047 and 1972 cm^{-1} indicate ^{13}CO ligands in natural abundance). The lack of other features in the ν_{CO} region, which would have been expected to indicate any bridging CO ligands, is consistent with the absence of rhodium clusters [14].

Data summarized in Table 1 show that the ν_{CO} bands of the rhodium carbonyls on the various supports are characterized by differing full-width at half-maximum (FWHM) values, indicating different degrees of uniformity of the supported species—and, by inference, different degrees of heterogeneity of the support surfaces. The zeolites, with spectra having the relatively sharp bands (FWHM < 5 cm^{-1}), are the supports with the most nearly uniform bonding sites for the rhodium. HY zeolite presents the most nearly uniform such sites, as expected [48]. The data point to multiple types of binding sites on the metal oxide supports.

Consistent with the IR results, the Rh K-edge EXAFS spectra give no evidence of Rh–Rh scattering paths (within error [49]) that would have indicated rhodium clusters (Table 2, Table S2, and Figures S10–S19); EXAFS data fitting led to models consistent with each rhodium atom bonded, on average, to two carbon atoms and two oxygen atoms on each support, in line with the symmetry indicated by the IR data and reports of $Rh(CO)_2$ on various supports (Table 1) [47,50–52].

The ν_{COsym} band position of the supported rhodium complexes (Table 1) show that it shifted to a higher energy as the electron-donor tendency of the support decreased. Correspondingly, X-ray Absorption Near Edge Spectra (XANES) indicate that the Rh K-edge energy (defined as the first maximum of the first derivative of the normalized absorbance with respect to beam energy) decreased with increasing ν_{COsym} values (Figure S20), confirming the decrease in electron density on rhodium with decreasing support electron-donor character [51,53].

3.2. Catalytic performance in acetylene semi-hydrogenation

The samples were investigated as catalysts for acetylene semi-hydrogenation at 373 K and 1 bar in a once-through plug-flow reactor. Each sample was first activated in flowing acetylene to convert the $Rh(CO)_2$ complexes into active species that incorporated acetylene ligands; IR spectra indicate that the ligand exchange was complete (Figure S21) and give no evidence of any feature that could be assigned to oligomers formed from acetylene, and thus we have no evidence to suggest that oligomers formed. Fitting a Rh–Rh first-shell scattering path on the EXAFS spectra of acetylene-activated samples (Table S3 and Figures S22–S27) resulted in nonsensical results indicating that there was an absence of rhodium clusters detectable with our methods. Furthermore, the data indicate that each rhodium atom was bonded to approximately four carbon atoms (in addition to two support oxygen atoms), consistent with two π-bonded acetylene ligands per rhodium atom.

Following the on-stream activation of the catalyst with acetylene, the feed to the flow reactor was switched to an equimolar acetylene + H_2 mixture flowing at steady state at 373 K at a gas hourly space velocity (GHSV) of 3000 mL $C_2H_2 \times g_{cat}^{-1} \times h^{-1}$. This value was chosen to give conversions that were shown to be differential (<2%) determining reaction rates (turnover frequencies, TOFs) directly. The data showing the

Table 1
ν_{COsym} and ν_{COasym} band positions characterizing supported $Rh(CO)_2$ complexes.

Support for rhodium dicarbonyl	ν_{COsym} (cm^{-1})	ν_{COasym} (cm^{-1})	FWHM[a] (cm^{-1})
HY zeolite	2117.7	2052.1	5/4
HY zeolite (DFT calculated)	2074.5	2008.4	–
Beta zeolite	2113.2	2048.3	18/12
SiO_2	2093.6	2029.9	22/14
γ-Al_2O_3	2085.9	2005.8	41/30
ZrO_2	2084.9	2011.6	31/36
Fe_2O_3	2080.1	2003.9	42/28
TiO_2	2083.9	2004.9	24/35
ZnO	2080.1	2003.9	23/38
MgO	2079.9	2002.7	31/27

[a] FWHM: Full width at half maximum; data characterize the symmetric and asymmetric bands, respectively.

Table 2
Summary of EXAFS best fit parameters characterizing samples prepared by adsorption of $Rh(CO)_2(acac)$ on zeolite and metal oxides having various electron-donor tendencies[a].

Sample	Shell [b]	*CN*	*R* (Å)	$\Delta\sigma^2 \times 10^3$ (Å^2)	ΔE_0 (eV)	*k* range (Å^{-1})	*R* range (Å)
$Rh(CO)_2$/HY zeolite	Rh–O_s	2.3 ± 0.1	2.11 ± 0.00	4.0 ± 0.3	2.89 ± 0.21	4.2–13.8	1.2–3.5
	Rh–C_{CO}	2.1 ± 0.1	1.87 ± 0.00	3.4 ± 0.4			
	Rh–O_{CO}	2.0 ± 0.2	2.99 ± 0.00	8.8 ± 1.1			
	Rh–O_{CO}*	4.0 ± 0.4	2.99 ± 0.00	1.9 ± 0.4			
	Rh–O_{CO}**	2.0 ± 0.2	2.99 ± 0.00	2.3 ± 0.6			
	Rh–Al	1.2 ± 0.1	3.15 ± 0.01	3.2 ± 0.9			
$Rh(CO)_2/SiO_2$	Rh–O_s	2.4 ± 0.1	2.05 ± 0.00	3.9 ± 0.4	−5.83 ± 0.37	3.9–14.5	1.2–4.0
	Rh–C_{CO}	2.0 ± 0.1	1.87 ± 0.00	2.3 ± 0.4			
	Rh–O_{CO}	1.9 ± 0.1	3.03 ± 0.00	5.9 ± 2.1			
	Rh–O_{CO}*	3.8 ± 0.2	3.03 ± 0.00	2.2 ± 0.4			
	Rh–O_{CO}**	1.9 ± 0.1	3.03 ± 0.00	4.4 ± 0.8			
	Rh–Si	1.3 ± 0.2	3.20 ± 0.01	4.1 ± 1.2			
$Rh(CO)_2$/ZnO	Rh–O_s	2.4 ± 0.1	2.07 ± 0.00	0.8 ± 0.2	2.51 ± 0.35	4.0–12.5	1.0–4.0
	Rh–C_{CO}	2.1 ± 0.2	1.97 ± 0.00	5.4 ± 0.9			
	Rh–O_{CO}	2.1 ± 0.1	3.02 ± 0.00	8.9 ± 2.8			
	Rh–O_{CO}*	4.2 ± 0.2	3.02 ± 0.00	0.4 ± 0.1			
	Rh–O_{CO}**	2.1 ± 0.1	3.02 ± 0.00	8.5 ± 0.6			
	Rh–Zn	0.8 ± 0.1	2.58 ± 0.01	9.2 ± 1.2			
$Rh(CO)_2$/MgO	Rh–O_s	1.9 ± 0.1	2.03 ± 0.00	5.2 ± 0.3	−9.62 ± 0.18	3.8–14.4	1.0–4.0
	Rh–C_{CO}	2.1 ± 0.1	1.84 ± 0.00	4.8 ± 0.3			
	Rh–O_{CO}	2.0 ± 0.2	2.99 ± 0.00	8.7 ± 1.4			
	Rh–O_{CO}*	4.2 ± 0.2	3.02 ± 0.00	5.5 ± 0.5			
	Rh–O_{CO}**	2.1 ± 0.1	3.02 ± 0.00	2.2 ± 0.2			
	Rh–Mg	0.7 ± 0.1	3.13 ± 0.01	1.8 ± 0.8			

[a] Notation: *CN*, coordination number; *R*, distance between absorber and backscatterer atoms; $\Delta\sigma^2$, mean square relative displacement; ΔE_0, inner potential correction. In this work, S_0^2 was taken to be 0.88 ± 0.03 (refined from fcc-rhodium reference provided in Figures S11 and S12).

[b] Rh–O_s denotes rhodium bonded to support surface oxygen atoms; Rh–C_{CO} and Rh–O_{CO} refer to carbon and oxygen atoms of carbonyl ligands bonded to rhodium, respectively; Rh–O_{CO}* refers to oxygen atoms of carbonyl ligands in Rh–C–O–Rh multiple scattering; Rh–O_{CO}** refers to oxygen atoms of carbonyl ligands in Rh–C–O–C–Rh multiple scattering.

conversions and selectivities of the catalysts incorporating the various supports under these conditions are shown in Fig. 1.

The activity and selectivity data characterizing rhodium on the various supports (Table 3) show that ethylene selectivity increased with decreasing electron density on the rhodium centers, controlled by the support electron-donor character (Fig. 2). Thus, the weak electron-donor support HY zeolite gave the maximum selectivity (92 % at a conversion of 1.1 % under conditions shown in Fig. 1). These results demonstrate that other than controlling the stability of the atomically dispersed supported metal catalysts [43], the electronic structure of the metal centers set by the electron-donor property of the support also plays an important role in controlling the product selectivities.

Measurements were made for comparison with catalysts incorporating small rhodium clusters, formed by reduction in flowing equimolar H_2 + helium mixtures at various temperatures, up to 573 K, for various times [54]. As shown by the data in Table 4 and Figures S28–S37, the first-shell Rh–Rh coordination number increased from 0.9 ± 0.2 to 6.6 ± 0.1 following the reduction. The average rhodium cluster diameter of Rh/HY zeolite-1.3 nm sample is estimated to be 1.3 nm, assuming a fcc-rhodium structure model [55], consistent with the STEM results (Figure S38) showing the average rhodium cluster diameter to be 1.1 ± 0.2 nm. We estimate the range in cluster diameters to be 0.5–1.3 nm in our samples incorporating supported rhodium clusters.

As shown in Fig. 3, HY zeolite-supported rhodium catalysts with various nuclearities exhibited significantly different catalytic performances in the acetylene hydrogenation reaction. Under our conditions, the rhodium clusters on HY zeolite were found to be much less selective for ethylene formation than the mononuclear rhodium complexes—and with higher initial activities. The conversion of mononuclear rhodium complexes to rhodium clusters led to an increase in the initial TOF from 16 to 46 (mol of C_2H_2 converted) × (Rh site × h)$^{-1}$ and to a decrease in ethylene selectivity from 92 % to 60 % (Figs. 3 and S39). Besides, the clusters were less stable than the mononuclear rhodium complexes—with deactivation of the clusters associated with coke formation made evident by the results of thermogravimetric analysis of used catalysts (Figure S40)—whereas, in contrast, the mononuclear HY zeolite-supported rhodium complex maintained its initial activity for as long as we kept it on stream (>30 h) with the equimolar feed composition at 373 K (Fig. 4).

Rh K-edge EXAFS data characterizing the used catalyst showed that the structure after 30 h of operation in the flow reactor ($Rh(C_2H_2)_2$/HY zeolite-postRXN) was approximately the same as that of the fresh activated catalyst ($Rh(C_2H_2)_2$/HY zeolite), with the rhodium still being atomically dispersed (Table 5, Figure S41 to S43). The best-fit model of the EXAFS data shows that each rhodium atom was bonded to approximately four carbon atoms and two oxygen atoms. These results demonstrate that under the reaction conditions, the $Rh(C_2H_2)_2$/HY zeolite catalyst retains its identity as a mononuclear metal complex, reflecting the strong resistance to sintering of the rhodium and the strong bonding of acetylene to the rhodium—consistent with the inference that these ligands are the predominant non-support ligands present during catalysis. Lack of any observable deactivation of the $Rh(C_2H_2)_2$/HY zeolite catalyst is consistent with the inference that coke formation was limited if it even occurred. This result might be associated with the lack of any observed selectivity for dimer formation on this catalyst, as oligomerization often leads to coke formation that deactivates conventional supported metal nanoparticle catalysts.

To further investigate the catalytic stability of the $Rh(C_2H_2)_2$/HY zeolite, we tested its performance under more severe conditions. As shown in Fig. 5, the experiment was initially conducted under the identical experimental conditions as shown in Fig. 1. Consistent with the results presented above, the ethylene selectivity was 92 % at an acetylene conversion of approximately 1 %. Subsequently, the feed gas was changed from equimolar acetylene and hydrogen to hydrogen-rich (C_2H_2:H_2 = 1:10 M) conditions at the same temperature (373 K). This change in hydrogen concentration led to an increase in acetylene conversion to 9.0 %. Data presented in Fig. 5 show that at this higher acetylene conversion in the presence of a hydrogen-rich feed, the ethylene selectivity remained approximately constant at 92 %. Next, we increased the temperature to 473 K at a ramp rate of 2 K/min keeping

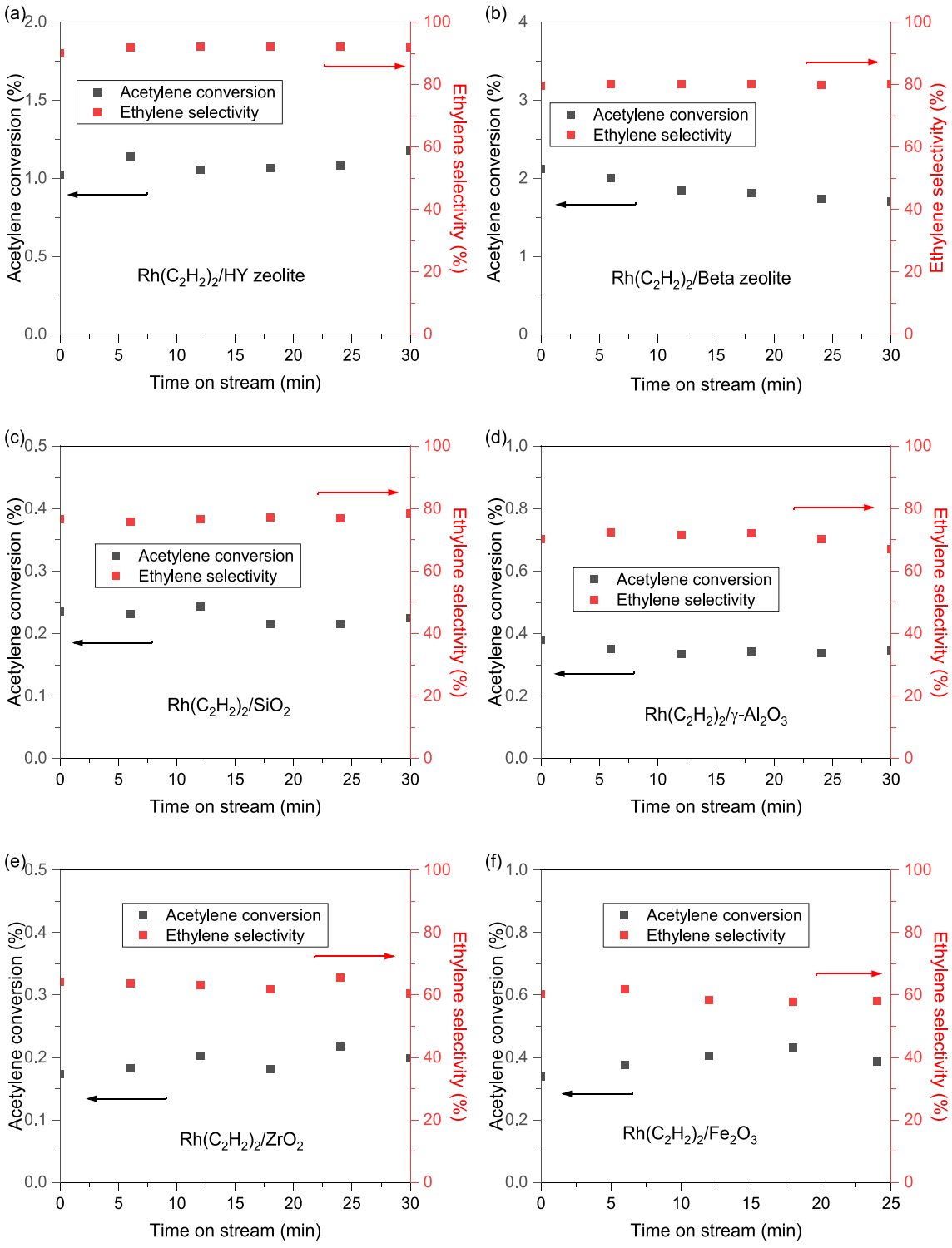

Fig. 1. Change in ethylene selectivity with time on stream characterizing acetylene hydrogenation on supported mononuclear rhodium complexes initially incorporating acetylene ligands. Reaction conditions: 100 mg of supported $Rh(CO)_2$ complex catalyst precursor was activated by exposure to acetylene at 373 K for 1 h, and then the feed gas was changed to 50 vol% C_2H_2, 50 vol% H_2, GHSV = 3000 mL(NTP) $C_2H_2 \times g_{cat}^{-1} \times h^{-1}$. The ethylene selectivity was recorded at 373 K; the conversion was < 2 %, and the pressure was 1 bar. This figure is continued on the following page.

the feed composition the same. During the ramp, the ethylene selectivity decreased slightly to 75 %, and the acetylene conversion increased to approximately 90 %. Once the reaction temperature had reached 473 K, the reactant composition was switched back to a C_2H_2:H_2 ratio of 1:1, and the reactor was quickly cooled to 373 K. The catalytic performance data collected subsequently at this condition indicate that the conversion and the selectivity were the same as those observed initially under the identical conditions (Fig. 5). These results suggest the lack of any significant changes in catalyst structure even under hydrogen-rich conditions at relatively high temperatures (473 K).

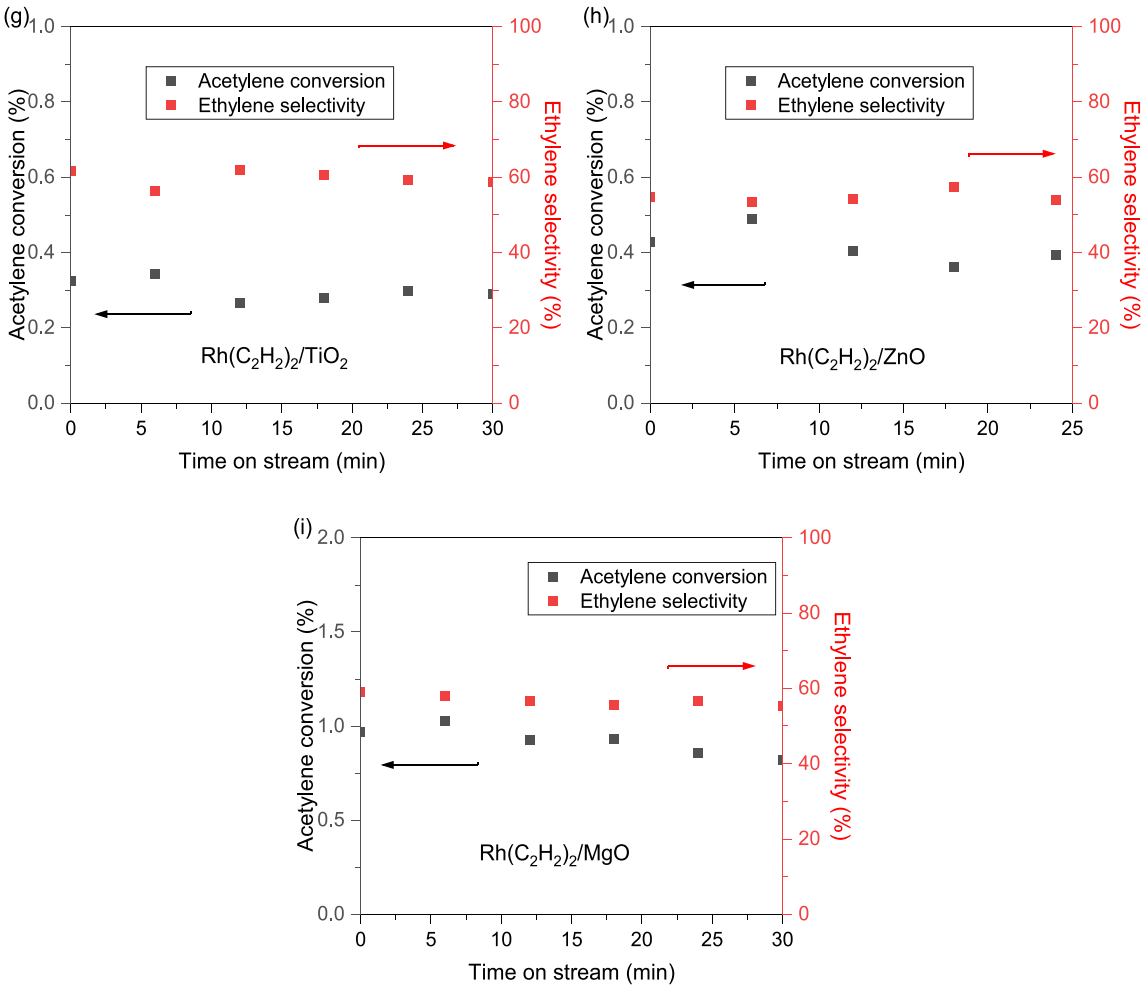

Fig. 1. (*continued*).

Table 3
Selectivities and TOF values characterizing the catalysts (initially incorporating supported $Rh(CO)_2$ complexes and exposed to acetylene at 373 K to replace the CO ligands with acetylene); data characterize acetylene hydrogenation at steady-state under differential conversion conditions at an C_2H_2/H_2 feed molar ratio of 1.0 at 373 K and 1 bar.

Catalyst precursor	C_2H_2 Conversion (%)	Selectivity (%)			TOF (h^{-1})[a]
		C_2H_4	C_2H_6	Dimers	
$Rh(C_2H_2)_2$/HY zeolite	1.1	91.9	8.1	0	16.4
$Rh(C_2H_2)_2$/Beta zeolite	1.9	80.1	18.3	1.6	21.6
$Rh(C_2H_2)_2/SiO_2$	0.3	74.9	17.2	7.9	2.9
$Rh(C_2H_2)_2/\gamma\text{-}Al_2O_3$	0.4	69.7	20.8	9.5	3.6
$Rh(C_2H_2)_2/ZrO_2$	0.2	62.1	23.2	14.6	2.5
$Rh(C_2H_2)_2/Fe_2O_3$	0.4	58.4	24.5	17.1	4.7
$Rh(C_2H_2)_2/TiO_2$	0.3	59.6	19.8	20.6	3.6
$Rh(C_2H_2)_2$/ZnO	0.4	55.2	18.1	26.7	5
$Rh(C_2H_2)_2$/MgO	1.0	58.0	19.2	22.8	12.6

[a] Turnover Frequency defined as: (number of C_2H_2 molecules converted) × (rhodium site × h)$^{-1}$.

To test for the possibility that ethane was a secondary product formed by hydrogenation of ethylene, experiments were performed with a reactor feed spiked with excess ethylene. The product analysis data show that ethylene formed as fast as acetylene was converted (Fig. 6). Correspondingly, the catalyst maintained the high ethylene selectivity (approximately 91 %) even when the feed composition was C_2H_2:C_2H_4:

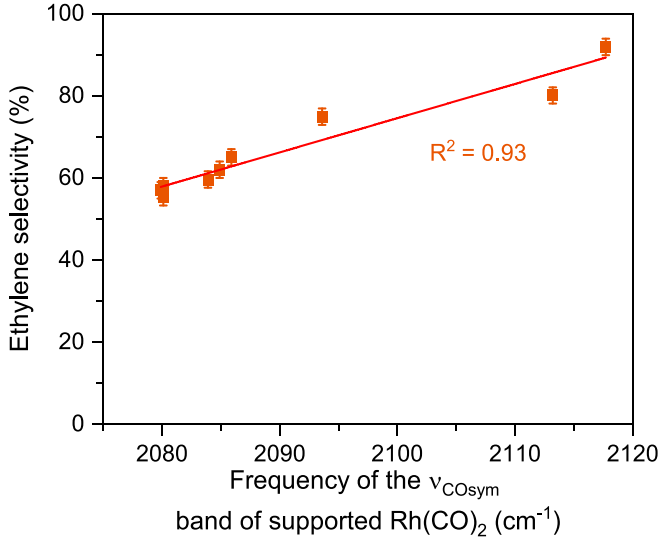

Fig. 2. Dependence of ethylene selectivity on the corresponding ν_{COsym} band position of the supported rhodium complexes. Each supported $Rh(CO)_2$ precursor was held for 1 h in flowing acetylene at 373 K and 1 bar, and then the feed gas composition was changed to C_2H_2:H_2 = 1:1 at the same temperature and pressure. GHSV was set to 3000 mL(NTP) $C_2H_2 \times g_{cat}^{-1} \times h^{-1}$ to ensure that acetylene conversions were differential (<2%).

Table 4
Summary of EXAFS best fit parameters characterizing Rh/HY zeolite samples with various rhodium nuclearities[a].

Sample	Shell [b]	*CN*	*R* (Å)	$\Delta\sigma^2 \times 10^3$ (Å^2)	ΔE_0 (eV)	*k* range (Å^{-1})	*R* range (Å)
Rh/HY zeolite-0.5 nm	Rh–O_s	2.0 ± 0.1	2.08 ± 0.00	2.8 ± 0.4	−2.14 ± 0.34	4.0–13.8	1.0–4.0
	Rh–Rh	0.9 ± 0.2	2.69 ± 0.01	9.6 ± 1.6			
	Rh–C_{CO}	2.1 ± 0.2	1.89 ± 0.01	8.1 ± 1.2			
	Rh–O_{CO}	1.9 ± 0.1	2.99 ± 0.00	9.8 ± 3.5			
	Rh–O_{CO}*	3.8 ± 0.2	2.99 ± 0.00	2.7 ± 0.4			
	Rh–O_{CO}**	1.9 ± 0.1	2.99 ± 0.00	9.3 ± 3.2			
	Rh–Al	1.0 ± 0.2	3.09 ± 0.01	4.0 ± 1.6			
Rh/HY zeolite-0.8 nm	Rh–O_s	1.2 ± 0.2	2.09 ± 0.00	3.5 ± 1.1	−3.04 ± 0.41	4.0–13.9	1.0–3.8
	Rh–Rh	4.0 ± 0.1	2.69 ± 0.00	3.2 ± 0.2			
	Rh–Rh_2	1.9 ± 0.3	3.80 ± 0.02	6.0 ± 1.5			
Rh/HY zeolite-1.0 nm	Rh–O_s	1.0 ± 0.2	2.07 ± 0.01	5.6 ± 1.9	−4.47 ± 0.29	4.0–13.9	1.0–3.8
	Rh–Rh	5.2 ± 0.1	2.69 ± 0.00	3.9 ± 0.1			
	Rh–Rh_2	2.5 ± 0.5	3.80 ± 0.01	6.6 ± 1.2			
Rh/HY zeolite-1.2 nm	Rh–O_s	0.8 ± 0.2	2.10 ± 0.01	2.0 ± 0.5	−3.24 ± 0.26	4.1–13.9	1.0–3.8
	Rh–Rh	6.2 ± 0.1	2.69 ± 0.00	3.8 ± 0.1			
	Rh–Rh_2	3.3 ± 0.6	3.80 ± 0.01	7.1 ± 1.1			
Rh/HY zeolite-1.3 nm	Rh–O_s	0.7 ± 0.2	2.07 ± 0.02	3.9 ± 0.9	−5.12 ± 0.25	4.1–13.9	1.0–3.8
	Rh–Rh	6.6 ± 0.1	2.69 ± 0.00	3.8 ± 0.1			
	Rh–Rh_2	3.7 ± 0.6	3.80 ± 0.01	7.2 ± 1.0			

[a] Notation: *CN*, coordination number; *R*, distance between the absorber and backscatterer atoms; $\Delta\sigma^2$, mean square relative displacement; ΔE_0, inner potential correction.

[b] Rh–O_s denote surface oxygen atoms of supports; Rh–C_{CO} and Rh–O_{CO} denote carbon and oxygen atoms of carbonyl ligands bonded to rhodium, respectively; Rh–O_{CO}* denotes oxygen atom of carbonyl ligands in Rh–C–O–Rh multiple scattering; Rh–O_{CO}** denotes oxygen atom of carbonyl ligands in Rh–C–O–C–Rh multiple scattering; Rh–Rh represents a first-shell Rh–Rh coordination; Rh–Rh_2 represents a second-shell Rh–Rh coordination.

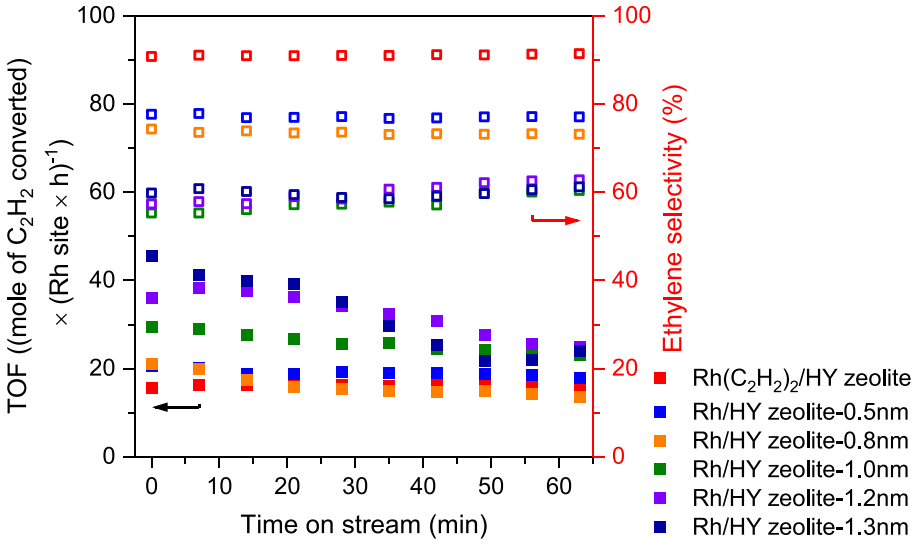

Fig. 3. Performance of HY zeolite-supported rhodium catalysts with various nuclearities for partial hydrogenation of acetylene. Conditions: feed, 50 vol% C_2H_2, 50 vol% H_2; temperature, 373 K; pressure, 1 bar; GHSV = 3000 mL(NTP) $C_2H_2 \times g_{cat}^{-1} \times h^{-1}$.

H_2 = 1:49:1 (corresponding to an acetylene conversion of > 98 % if the feed had been just acetylene + H_2). Consistent with these results, when a pulse of acetylene was injected into a flowing ethylene + H_2 stream when ethylene hydrogenation was taking place (catalyzed by the HY zeolite-supported rhodium complex initially having ethylene ligands only (in addition to the support)), the ethylene conversion decreased sharply (Figure S44). Thus, we hypothesized that acetylene bonded more strongly to rhodium than ethylene, rapidly displacing it, consistent with the lack of inhibition of acetylene hydrogenation by ethylene and explaining (at least in part) the high selectivity of the catalyst for acetylene hydrogenation without secondary ethylene hydrogenation.

3.3. Mechanistic insights from DFT calculations

To provide insights into the chemistry, we performed electronic structure calculations at the level of density functional theory (DFT), PBE/6–31 + G(d,p) (LANL2DZ for Rh)[41–43] (details in Section S10 of Supporting Information), investigating various possible pathways for the conversion of acetylene into the primary products on the zeolite-supported catalyst, including elementary steps involving the breaking of a bond between rhodium and support oxygen, as inferred to be significant for ethylene hydrogenation by Vummaleti et al. (Fig. 7) [56,57]. The catalyst precursor was modeled as a *cis*-Rh$(C_2H_2)_2$ complex, **1** (Figure S45), with a square-planar coordination formed by two zeolite framework oxygen atoms and two acetylene ligands anchored at the middle of the two four-rings facing the zeolite supercage (33 T cluster model with a total of 13 interconnected four-rings). This model was validated by calculating ν_{CO} band positions characterizing a Rh$(CO)_2$ complex at the same position (comparison shown in Table 1). The corresponding Gibbs reaction and activation energies at 373 K are presented in Fig. 7, where it is demonstrated that the reaction starts with the coordination of H_2 to a rhodium center **1** in a side-on fashion. η^2-H_2 leads to complex **2**, $[Rh(C_2H_2)_2(H_2)]^+$, with a free energy change of 14.9 kcal/mol. Complex **2** undergoes oxidative addition of H_2 forming

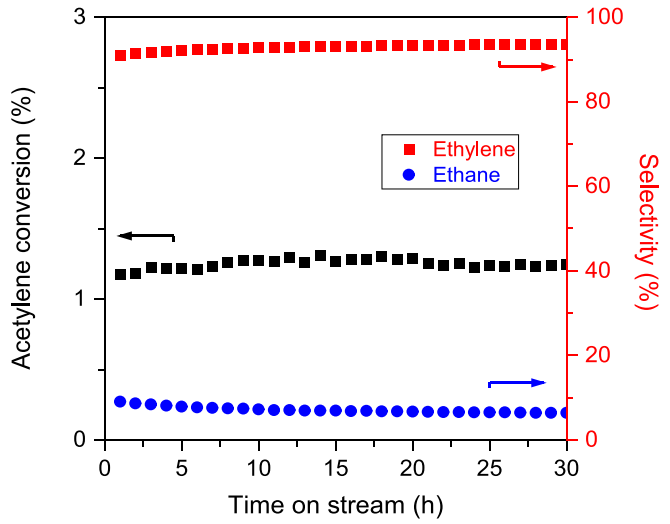

Fig. 4. Acetylene hydrogenation on catalyst initially present as $Rh(C_2H_2)_2$/HY zeolite in a flow reactor with an equimolar $C_2H_2 + H_2$ feed at 373 K (GHSV = 3000 mL(NTP) of $C_2H_2 \times g_{cat}^{-1} \times h^{-1}$).

the octahedral *cis*-dihydride complex **3**, $[Rh(C_2H_2)_2(H)_2]^+$. Next, acetylene in **3** undergoes hydrogenation leading to the more stable ethylenyl complex **4**, $[Rh(C_2H_2)(C_2H_3)(H)]^+$. In the next step, the hydrogenation of the ethylenyl in **4** yields complex **5** $[Rh(C_2H_2)(C_2H_4)]^+$ with ethylene coordinated to the rhodium center. Complex **5** is a branch point: H_2 or C_2H_2 can interact with the support yielding **6** or **9**, respectively. Then, H_2 and C_2H_2 in complexes **6** and **9**, respectively, can attack the metal center forming complex **7** ($\Delta G^{\neq} = 6.5$ kcal/mol) and the three-ligand complex **10** ($\Delta G^{\neq} = 4.5$ kcal/mol). Complex **5** plays a role on the fate of the reaction: the difference in free energies of these two possible routes ($\Delta\Delta G^{\neq} = 2$ kcal/mol) determines the selectivity towards addition of C_2H_2 versus H_2. Hence, the **5** → **9** → **10** path is preferred over the **6** → **7** → **8** path; the former ends up with C_2H_4 elimination, whereas the latter yields C_2H_6. We have also considered H_2 addition to complex **10** to understand how the presence of three ligands (two C_2H_2 and one C_2H_4) affects selectivity. The resulting branch point **11**, corresponding to $[Rh(C_2H_2)_2(C_2H_4)]^+$ with η^2-H_2, can undergo oxidative addition yielding **11** → **17** ($\Delta G^{\neq} = 9.1$ kcal/mol), which is preferred over **11** → **2** ($\Delta G^{\neq} = 10.8$ kcal/mol) and **11** → **12** ($\Delta G^{\neq} = 11.5$ kcal/mol): The **11** → **2** step refers to C_2H_4 elimination, and **11** → **12** reflects the bond rupture between rhodium and the support. Complex **17** $[Rh(C_2H_2)_2(C_2H_4)(H)_2]^+$ would easily undergo acetylene hydrogenation (**17** → **19**, $\Delta G^{\neq} = 3.1$ kcal/mol), rather than ethylene hydrogenation (**17** → **18**, $\Delta G^{\neq} = 5.7$ kcal/mol); the **17** → **18** → **16** path would lead to the formation of C_2H_6. The aforementioned scenario (formation of **17**) might hold depending on the nature of the metal, the ligands, and the support; if that were the case, C_2H_4 and C_2H_6 would have been eliminated from **19** and **16**, respectively. In the current case, steps **5** → **6** → **7** and **5** → **9** → **10** are the major paths yielding ethane and ethylene, respectively, and they primarily determine the selectivity (the branch points **10**, **11**, **17**, and **19**

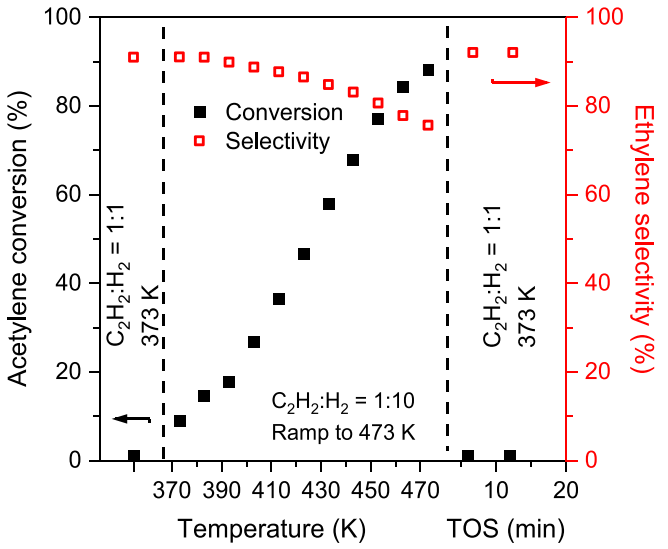

Fig. 5. Comparison of the performance of the catalyst initially present as $Rh(C_2H_2)_2$/HY zeolite in flowing 50 vol% C_2H_2, 50 vol% H_2 at 373 K and 1 bar and at a GHSV = 3000 mL(NTP) of $C_2H_2 \times g_{cat}^{-1} \times h^{-1}$ before and after exposure to a temperature ramp from 373 to 473 K at a ramp rate of 2 K/min with the catalyst in flowing 5 vol% C_2H_2, 50 vol% H_2, balanced with helium at a GHSV = 120 mL (NTP) of $C_2H_2 \times g_{cat}^{-1} \times h^{-1}$. See text for details.

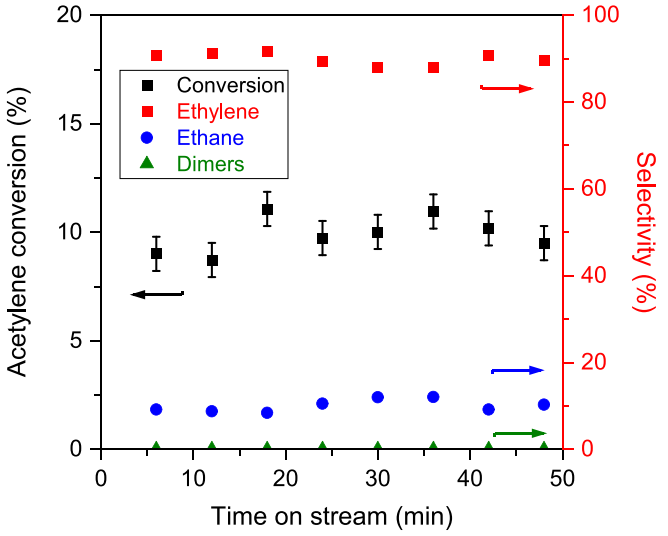

Fig. 6. Performance of catalyst when the feed was acetylene + ethylene + H_2 (C_2H_2:C_2H_4:H_2 = 1:49:1) at a total gas flow rate of 102 mL (NTP)/min with 500 mg of catalyst containing 1.0 wt% rhodium at 373 K.

Table 5
Summary of EXAFS best fit parameters characterizing $Rh(C_2H_2)_2$/HY zeolite sample before catalysis and after 30 h of reaction.[a]

Sample	Shell[b]	*CN*	*R* (Å)	$\Delta\sigma^2 \times 10^3$ (Å^2)	ΔE_0 (eV)	*k* range (Å^{-1})	*R* range (Å)
$Rh(C_2H_2)_2$/HY zeolite	Rh–O_s	2.3 ± 0.1	2.10 ± 0.00	1.3 ± 0.3	5.10 ± 0.27	3.6–13.0	1.0–3.0
	Rh–C	4.3 ± 0.2	2.24 ± 0.00	1.7 ± 0.3			
	Rh–Al	1.0 ± 0.2	3.05 ± 0.01	5.7 ± 1.9			
$Rh(C_2H_2)_2$/HY zeolite-postreaction	Rh–O_s	2.2 ± 0.1	2.10 ± 0.00	1.7 ± 0.3	5.24 ± 0.24	3.7–13.7	1.0–3.0
	Rh–C	4.3 ± 0.1	2.23 ± 0.00	1.0 ± 0.2			
	Rh–Al	1.0 ± 0.1	3.05 ± 0.01	5.4 ± 1.8			

[a] Notation: *CN*, coordination number; *R*, distance between the absorber and backscatterer atoms; $\Delta\sigma^2$, mean square relative displacement; ΔE_0, inner potential correction.
[b] Rh–O_s denotes bonding of rhodium to support surface oxygen atoms; Rh–C denotes bonding of rhodium to carbon atom of acetylene ligands.

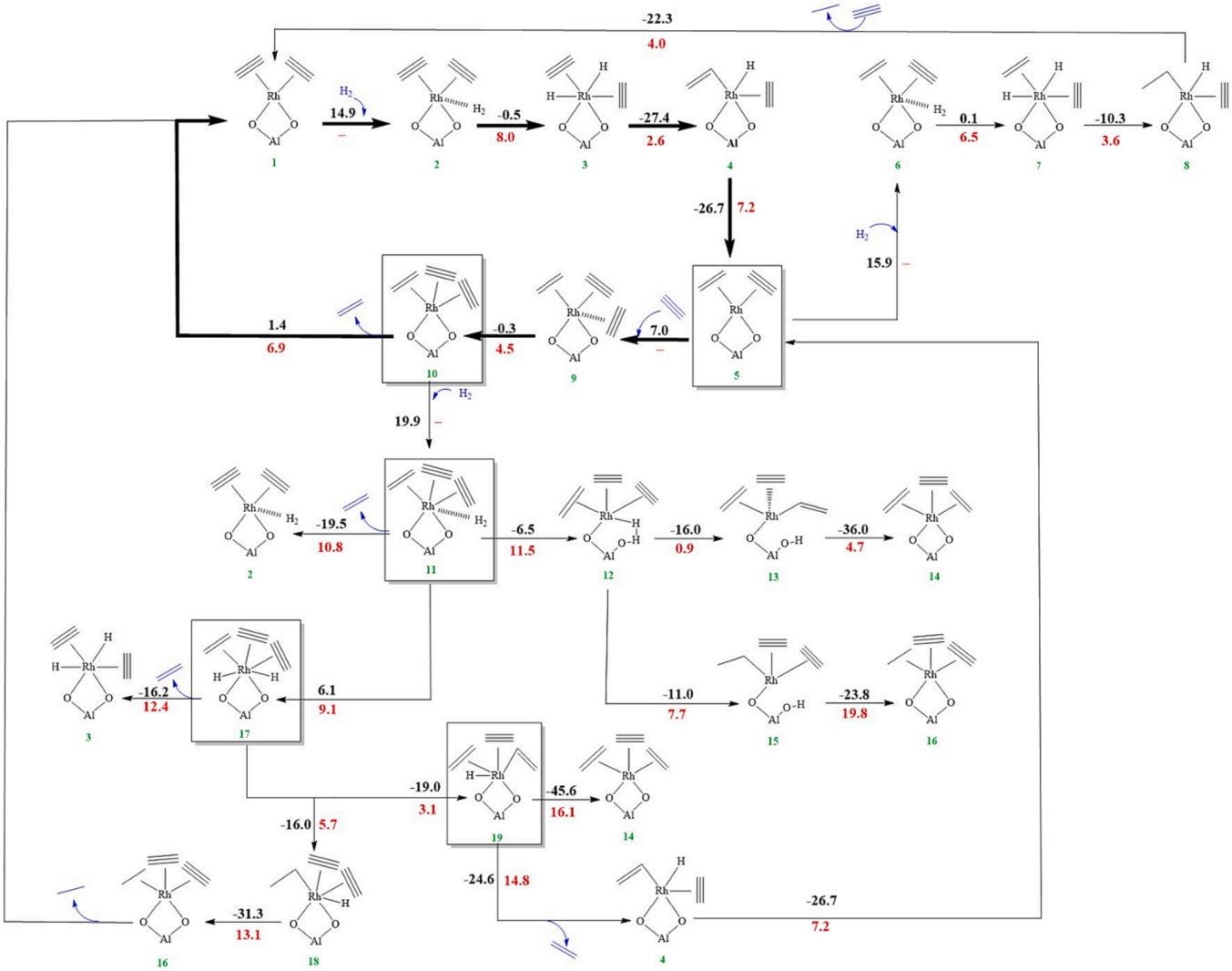

Fig. 7. Mechanism of acetylene hydrogenation starting from the HY zeolite-supported rhodium complex **1**, $[Rh(C_2H_2)_2]^+$. Gibbs reaction and activation energies (in kcal/mol calculated at 373 K) of individual steps are given in **black** and **red**, respectively. Bold arrows indicate the preferred pathway with the lowest barriers.

are inferred to contribute minimally to the ethylene formation, as determined by the energetics). The difference between the barriers characterizing **9** → **10** and **6** → **7** implies a ratio of rate constants (k_1/k_2) yielding ethylene and ethane of approximately 14.9, which is in good agreement with the observation (characterized by a corresponding ratio of 15.6 (Table S4)).

3.4. *Influence of electronic structure on catalyst performance*

We determined thorough catalyst performance data for the two supported mononuclear rhodium catalysts having the supports with the most widely different electron-donor properties (HY zeolite and MgO). The selectivity vs. conversion data extrapolated to zero conversion (Figure S46) demonstrate that both ethylene and ethane are primary products, formed on each catalyst, thus confirming the conclusion stated above that ethane formation as a secondary product is not a kinetically significant reaction.

4. Discussion

A central result of this work is that selective semi-hydrogenation of acetylene catalyzed by the supported mononuclear rhodium complexes is strongly influenced by the support—as a ligand. To quantify the ligand effect, we used the kinetics data obtained with acetylene + H_2 feeds at low acetylene conversions (<0.3 %) (Table S4) and represented the kinetics in a simplified way, approximating the parallel reactions to form ethylene and ethane formation with first-order kinetics, representing the respective rate constants as k_1 and k_2 (Fig. 8; separate experiments showed that first-order kinetics represented the data well). Thus, we determined how the k_1/k_2 ratio depends on the electron-donor properties of the supports by using the ν_{COsym} band positions of the precursor $Rh(CO)_2$ complexes as a correlating parameter—thereby determining the ligand effects of supports having strong, moderate, and weak electron-donor character (MgO, SiO_2, and HY zeolite, respectively)—the results of charge analyses performed on the corresponding $Rh(CO)_2$ complexes present on these supports (Figure S47) confirm this trend, as presented in Table S5.

The data (Fig. 8) demonstrate a marked ligand effect on the catalyst selectivity, providing a basis for selection of supports to maximize selectivity.

Thus, the results presented here point the way to the choice of supports for mononuclear rhodium complex catalysts for selective acetylene semi-hydrogenation. Because of its commercial importance, this reaction has long been an important research topic in catalysis, but rhodium has drawn little attention because it has been considered to be unselective. The results presented here show that stabilization of rhodium as

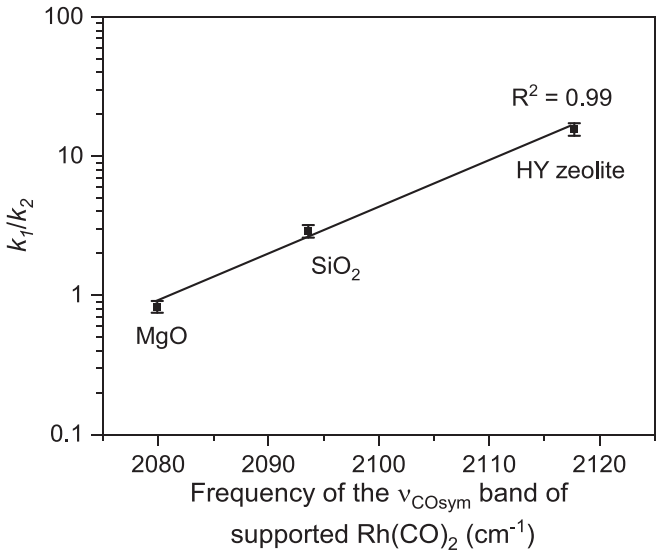

Fig. 8. Ligand effect in the selective semi-hydrogenation catalysis: dependence of k_1/k_2 ratio on the corresponding ν_{COsym} band position of the unused catalyst before replacement of CO ligands with C_2H_2.

mononuclear species on supports with low electron-donor tendencies opens the door to stable, selective acetylene semi-hydrogenation catalysts. The supported rhodium species need to be resistant to sintering for stable, selective catalysis.

We recognize a tradeoff in the structure of the rhodium catalyst. The selectivity comes at a cost: the activity of rhodium clusters exceeds that of the mononuclear rhodium complexes [29,58,59]. Nonetheless, the comparison presented in Table S6 indicates that the mononuclear zeolite-supported catalyst is unique among rhodium catalysts in offering a semi-hydrogenation selectivity and stability comparable to those of the best-performing catalysts with noble metals known to offer high selectivity, such as palladium. We further note that because rhodium is expensive, it is advantageous to use it at the highest possible dispersion.

5. Conclusions

The results presented here demonstrate how tuning of the electronic properties of mononuclear rhodium by choice of the solid support as a ligand affords selective acetylene semi-hydrogenation catalysts. The HY zeolite-supported rhodium complex is stable in flow-reactor operation at 373 K in an ethylene-rich environment, with an ethylene selectivity > 90 %, even when ethylene is present in a large excess over acetylene. These results point to the potential practical value of supported rhodium complexes as semi-hydrogenation catalysts.

Declaration of Competing Interest

The authors declare that they have no known competing financial interests or personal relationships that could have appeared to influence the work reported in this paper.

Data availability

Data will be made available on request.

Acknowledgments

The work at Koç University was supported by Koç University TUPRAS Energy Center (KUTEM). A.U. thanks the Fulbright Türkiye's Visiting Scholar Program and the TUBA-GEBIP Award of the Turkish Academy of Sciences. Y.Z. acknowledges the Fung Scholarship. We acknowledge the use of STEM services and facilities of the Central Research Infrastructure Directorate at Koç University. Computing resources performed in the investigation were provided by the National Center for High Performance Computing of Turkey (UHEM) under grant number 1006502019 and by TUBITAK ULAKBIM, High Performance and Grid Computing Center (TRUBA resources) and the Texas Advanced Computing Center (TACC) at The University of Texas at Austin. M.Y. and V.A. thank TUBITAK (Project Number: 121Z092); T.A. thanks the Welch Foundation (Grant No. BX-0048) for support. Work at the Stanford Synchrotron Radiation Light source of the SLAC National Accelerator Laboratory was supported by the U.S. Department of Energy (DOE), Office of Science, Basic Energy Sciences (BES), under Contract DE-AC02-76SF00515 and by Co-ACCESS, supported by DOE BES, Chemical Sciences, Geosciences, and Biosciences Division, which also supported the work at the University of California (B.C.G.; DEFG02-04ER15513).

Appendix A. Supplementary material

Supplementary data to this article can be found online at https://doi.org/10.1016/j.jcat.2023.115196.

References

[1] L. Liu, A. Corma, Metal catalysts for heterogeneous catalysis: from single atoms to nanoclusters and nanoparticles, Chem. Rev. 118 (2018) 4981–5079.
[2] G. Kyriakou, M.B. Boucher, A.D. Jewell, E.A. Lewis, T.J. Lawton, A.E. Baber, H. L. Tierney, M. Flytzani-Stephanopoulos, E.C. Sykes, Isolated metal atom geometries as a strategy for selective heterogeneous hydrogenations, Science 335 (2012) 1209–1212.
[3] J. Liu, Catalysis by supported single metal atoms, ACS Catal. 7 (2017) 34–59.
[4] Z.-Y. Li, Z. Yuan, X.-N. Li, Y.-X. Zhao, S.-G. He, CO oxidation catalyzed by single gold atoms supported on aluminum oxide clusters, J. Am. Chem. Soc. 136 (2014) 14307–14313.
[5] G. Malta, S.A. Kondrat, S.J. Freakley, C.J. Davies, L. Lu, S. Dawson, A. Thetford, E. K. Gibson, D.J. Morgan, W. Jones, P.P. Wells, P. Johnston, R. Catlow, C.J. Kiely, G. J. Hutchings, Identification of single-site gold catalysis in acetylene hydrochlorination, Science 355 (2017) 1399–1403.
[6] M. Flytzani-Stephanopoulos, Gold atoms stabilized on various supports catalyze the water–gas shift reaction, Acc. Chem. Res. 47 (2014) 783–792.
[7] A.S.K. Hashmi, G.J. Hutchings, Gold catalysis, Angew. Chem. Int. Ed. 45 (2006) 7896–7936.
[8] I. Ro, J. Qi, S. Lee, M. Xu, X. Yan, Z. Xie, G. Zakem, A. Morales, J.G. Chen, X. Pan, D.G. Vlachos, S. Caratzoulas, P. Christopher, Bifunctional hydroformylation on heterogeneous Rh-WO_x pair site catalysts, Nature 609 (2022) 287–292.
[9] M.G. Farpón, W. Henao, P.N. Plessow, E. Andrés, R. Arenal, C. Marini, G. Agostini, F. Studt, G. Prieto, Rhodium single-atom catalyst design through oxide support modulation for selective gas-phase ethylene hydroformylation, Angew. Chem. Int. Ed. 135 (2023) e202214048.
[10] L. Qi, S. Das, Y. Zhang, D. Nozik, B.C. Gates, A.T. Bell, Ethene hydroformylation catalyzed by rhodium dispersed with zinc or cobalt in silanol nests of dealuminated zeolite beta, J. Am. Chem. Soc. 145 (2023) 2911–2929.
[11] L. Lin, S. Yao, R. Gao, X. Liang, Q. Yu, Y. Deng, J. Liu, M. Peng, Z. Jiang, S. Li, A highly CO-tolerant atomically dispersed Pt catalyst for chemoselective hydrogenation, Nat. Nanotechnol. 14 (2019) 354–361.
[12] X. Ye, C. Yang, X. Pan, J. Ma, Y. Zhang, Y. Ren, X. Liu, L. Li, Y. Huang, Highly selective hydrogenation of CO_2 to ethanol via designed bifunctional Ir_1–In_2O_3 single-atom catalyst, J. Am. Chem. Soc. 142 (2020) 19001–19005.
[13] H. Yan, H. Cheng, H. Yi, Y. Lin, T. Yao, C. Wang, J. Li, S. Wei, J. Lu, Single-atom Pd_1/graphene catalyst achieved by atomic layer deposition: remarkable performance in selective hydrogenation of 1,3-butadiene, J. Am. Chem. Soc. 137 (2015) 10484–10487.
[14] J. Shan, M. Li, L.F. Allard, S. Lee, M. Flytzani-Stephanopoulos, Mild oxidation of methane to methanol or acetic acid on supported isolated rhodium catalysts, Nature 551 (2017) 605–608.
[15] H. Li, M. Fei, J.L. Troiano, L. Ma, X. Yan, P. Tieu, Y. Yuan, Y. Zhang, T. Liu, X. Pan, G.W. Brudvig, D. Wang, Selective Methane Oxidation by Heterogenized Iridium Catalysts, J. Am. Chem. Soc. 145 (2023) 769–773.
[16] D. Liu, Q. He, S. Ding, L. Song, Structural regulation and support coupling effect of single-atom catalysts for heterogeneous catalysis, Adv. Energy Mater. 10 (2020) 2001482.
[17] J.A. Osborn, F.H. Jardine, J.F. Young, G. Wilkinson, The preparation and properties of tris(triphenylphosphine)halogenorhodium(I) and some reactions thereof including catalytic homogeneous hydrogenation of olefins and acetylenes and their derivatives, J. Chem. Soc. A: Inorg., Phys., Theoret. (1966) 1711–1732.
[18] D. Koch, W. Leitner, Rhodium-catalyzed hydroformylation in supercritical carbon dioxide, J. Am. Chem. Soc. 120 (1998) 13398–13404.
[19] C.M. Thomas, G. Süss-Fink, Ligand effects in the rhodium-catalyzed carbonylation of methanol, Coord. Chem. Rev. 243 (2003) 125–142.

[20] W. Shang, M. Gao, Y. Chai, G. Wu, N. Guan, L. Li, Stabilizing isolated rhodium cations by MFI zeolite for heterogeneous methanol carbonylation, ACS Catal. 11 (2021) 7249–7256.
[21] R.A. Peralta, M.T. Huxley, J.D. Evans, T. Fallon, H. Cao, M. He, X.S. Zhao, S. Agnoli, C.J. Sumby, C.J. Doonan, Highly active gas phase organometallic catalysis supported within metal–organic framework pores, J. Am. Chem. Soc. 142 (2020) 13533–13543.
[22] J. Amsler, B.B. Sarma, G. Agostini, G. Prieto, P.N. Plessow, F. Studt, Prospects of heterogeneous hydroformylation with supported single atom catalysts, J. Am. Chem. Soc. 142 (2020) 5087–5096.
[23] R. Lang, T. Li, D. Matsumura, S. Miao, Y. Ren, Y.T. Cui, Y. Tan, B. Qiao, L. Li, A. Wang, X. Wang, T. Zhang, Hydroformylation of olefins by a rhodium single-atom catalyst with activity comparable to $RhCl(PPh_3)_3$, Angew. Chem. Int. Ed. 55 (2016) 16054–16058.
[24] F. Studt, F. Abild-Pedersen, T. Bligaard, R.Z. Sørensen, C.H. Christensen, J. K. Nørskov, Identification of non-precious metal alloy catalysts for selective hydrogenation of acetylene, Science 320 (2008) 1320–1322.
[25] R. Shi, Z. Wang, Y. Zhao, G.I.N. Waterhouse, Z. Li, B. Zhang, Z. Sun, C. Xia, H. Wang, T. Zhang, Room-temperature electrochemical acetylene reduction to ethylene with high conversion and selectivity, Nat. Catal. 4 (2021) 565–574.
[26] A. Borodziński, G. Bond, Selective hydrogenation of ethyne in ethene-rich streams on palladium catalysts. Part 1. Effect of changes to the catalyst during reaction, Catal. Rev. Sci. Eng. 48 (2006) 91–144.
[27] X. Shi, Y. Lin, L. Huang, Z. Sun, Y. Yang, X. Zhou, E. Vovk, X. Liu, X. Huang, M. Sun, S. Wei, J. Lu, Copper Catalysts in Semihydrogenation of Acetylene: From Single Atoms to Nanoparticles, ACS Catal. 10 (2020) 3495–3504.
[28] Z.J. Zhao, J. Zhao, X. Chang, S. Zha, L. Zeng, J. Gong, Competition of C–C bond formation and C−H bond formation For acetylene hydrogenation on transition metals: A density functional theory study, Am. Inst. Chem. Eng. J. 65 (2018) 1059–1066.
[29] G. Bond, P. Wells, The hydrogenation of acetylene: II. The reaction of acetylene with hydrogen catalyzed by alumina-supported palladium, J. Catal. 5 (1966) 65–73.
[30] A. Hoffman, L. Debefve, A. Bendjeriou-Sedjerari, S. Ould-Chikh, S.R. Bare, J.-M. Basset, B.C. Gates, Transmission and fluorescence X-ray absorption spectroscopy cell/flow reactor for powder samples under vacuum or in reactive atmospheres, Rev. Sci. Instrum. 87 (2016), 073108.
[31] B. Ravel, M. Newville, ATHENA, ARTEMIS, HEPHAESTUS: data analysis for X-ray absorption spectroscopy using IFEFFIT, J. Synchrotron Radiat. 12 (2005) 537–541.
[32] S. Zabinsky, J. Rehr, A. Ankudinov, R. Albers, M. Eller, Multiple-scattering calculations of X-ray-absorption spectra, Phys. Rev. B 52 (1995) 2995.
[33] M.M. Conradie, J. Conradie, Solid state packing of $[Rh(\beta\text{-diketonato})(CO)_2]$ complexes. Crystal structure of $[Rh(PhCOCHCOC_4H_3S)(CO)_2]$, J. Mol. Struct. 1051 (2013) 137–143.
[34] M. Bühl, M. Håkansson, A.H. Mahmoudkhani, L. Öhrström, X-ray structures and DFT calculations on rhodium−olefin complexes: comments on the ^{103}Rh NMR shift−stability correlation, Organometallics 19 (2000) 5589–5596.
[35] P.W. Kletnieks, A.J. Liang, R. Craciun, J.O. Ehresmann, D.M. Marcus, V.A. Bhirud, M.M. Klaric, M.J. Hayman, D.R. Guenther, O.P. Bagatchenko, D.A. Dixon, B. C. Gates, J.F. Haw, Molecular heterogeneous catalysis: a single-site zeolite-supported rhodium complex for acetylene cyclotrimerization, Chem. Eur. J. 13 (2007) 7294–7304.
[36] M. Babucci, C.Y. Fang, J.E. Perez-Aguilar, A.S. Hoffman, A. Boubnov, E. Guan, S. R. Bare, B.C. Gates, A. Uzun, Controlling catalytic activity and selectivity for partial hydrogenation by tuning the environment around active sites in iridium complexes bonded to supports, Chem. Sci. 10 (2019) 2623–2632.
[37] F.W. Lytle, D.E. Sayers, E.A. Stern, Report of the international workshop on standard and criteria in x-ray absorption spectoroscopy, Phys. B 158 (1989) 701–722.
[38] M. Frisch, G. Trucks, H. Schlegel, G. Scuseria, M. Robb, J. Cheeseman, G. Scalmani, V. Barone, G. Petersson, H. Nakatsuji, X. Li, M. Caricato, A. Marenich, J. Bloino, B. Janesko, R. Gomperts, B. Mennucci, H. Hratchian, J. V., D. J. F., Gaussian 16, Revision C. 01. Gaussian, Inc., Wallingford CT. 2016.
[39] J.P. Perdew, K. Burke, M. Ernzerhof, Generalized gradient approximation made simple, Phys. Rev. Lett. 77 (1996) 3865.
[40] J. Perdew, K. Burke, M. Ernzerhof, Errata: Generalized gradient approximation made 521 simple, Phys. Rev. Lett. 78 (1997) 522.
[41] P.J. Hay, W.R. Wadt, *Ab initio* effective core potentials for molecular calculations. Potentials for K to Au including the outermost core orbitals, J. Chem. Phys. 82 (1985) 299–310.
[42] M. McKee, S. Worley, A theoretical study of rhodium/carbonyl species, Chem. A Eur. J. 92 (1988) 3699–3700.
[43] S.F. Kurtoğlu, A.S. Hoffman, D. Akgül, M. Babucci, V. Aviyente, B.C. Gates, S. R. Bare, A. Uzun, Electronic structure of atomically dispersed supported iridium catalyst controls iridium aggregation, ACS Catal. 10 (2020) 12354–12358.
[44] D. Akgül, S.F. Kurtoğlu-Öztulum, Y. Zhao, V. Fındık, A. Monari, A. Uzun, V. Aviyente, Influence of ionic liquids on the electronic environment of atomically dispersed Ir on (MgO)(100), PCCP 24 (2022) 11305–11314.
[45] K.B. Wiberg, P.R. Rablen, Atomic charges, J. Org. Chem. 83 (2018) 15463–15469.
[46] J. Lu, C. Aydin, N.D. Browning, B.C. Gates, Oxide-and zeolite-supported isostructural $Ir(C_2H_4)_2$ complexes: molecular-level observations of electronic effects of supports as ligands, Langmuir 28 (2012) 12806–12815.
[47] C. Martinez-Macias, P. Serna, B.C. Gates, Isostructural zeolite-supported rhodium and iridium complexes: tuning catalytic activity and selectivity by ligand modification, ACS Catal. 5 (2015) 5647–5656.
[48] J.F. Goellner, B.C. Gates, G.N. Vayssilov, N. Rösch, Structure and bonding of a site-isolated transition metal complex: Rhodium dicarbonyl in highly dealuminated zeolite Y, J. Am. Chem. Soc. 122 (2000) 8056–8066.
[49] J. Finzel, K.M. Sanroman Gutierrez, A.S. Hoffman, J. Resasco, P. Christopher, S. R. Bare, Limits of detection for EXAFS characterization of heterogeneous single-atom catalysts, ACS Catal. 13 (2023) 6462–6473.
[50] K. Khivantsev, A. Vityuk, H.A. Aleksandrov, G.N. Vayssilov, O.S. Alexeev, M. D. Amiridis, Effect of Si/Al ratio and Rh precursor used on the synthesis of HY zeolite-supported rhodium carbonyl hydride complexes, J. Phys. Chem. C 119 (2015) 17166–17181.
[51] P. Serna, D. Yardimci, J.D. Kistler, B.C. Gates, Formation of supported rhodium clusters from mononuclear rhodium complexes controlled by the support and ligands on rhodium, PCCP 16 (2014) 1262–1270.
[52] Q. Zhang, S. Gao, J. Yu, Metal sites in zeolites: synthesis, characterization, and catalysis, Chem. Rev. 123 (2023) 6039–6106.
[53] D. Yardimci, P. Serna, B.C. Gates, Tuning catalytic selectivity: zeolite- and magnesium oxide-supported molecular rhodium catalysts for hydrogenation of 1,3-butadiene, ACS Catal. 2 (2012) 2100–2113.
[54] D. Yang, P. Xu, N.D. Browning, B.C. Gates, Tracking Rh atoms in zeolite HY: First steps of metal cluster formation and influence of metal nuclearity on catalysis of ethylene hydrogenation and ethylene dimerization, J. Phys. Chem. Lett. 7 (2016) 2537–2543.
[55] J. van Zon, D. Koningsberger, H. van't Blik, D. Sayers, An EXAFS study of the structure of the metal–support interface in highly dispersed Rh/Al_2O_3 catalysts, J. Chem. Phys. 82 (1985) 5742–5754.
[56] S.V. Vummaleti, A. Genest, N. Kuriakose, N. Rösch, Ethene Dimerization and Hydrogenation over a Zeolite-Supported Rh(I)-Carbonyl Complex: Mechanistic Insights from DFT Modeling, ACS Catal. 8 (2018) 9836–9846.
[57] S.V. Vummaleti, N. Kuriakose, S. Dinda, Y. Wu, A. Genest, N. Rösch, C–C coupling at a zeolite-supported Rh(I) complex. DFT search for the mechanism, Catal. Sci. Technol. 9 (2019) 2781–2793.
[58] J. Sheridan, W. Reid, The metal-catalysed reaction between acetylene and hydrogen. Part VI. The reaction over rhodium and iridium, J. Chem. Soc. A: Inorg., Phys., Theoret. 6 (1952) 2962–2966.
[59] A.S. Al-Ammar, G. Webb, Hydrogenation of acetylene over supported metal catalysts. Part 3.—$[^{14}C]$ tracer studies of the effects of added ethylene and carbon monoxide on the reaction catalysed by silica-supported palladium, rhodium and iridium, J. Chem. Soc. Faraday Trans. 1: Phys. Chem. Conden. Phases 75 (1979) 1900–1911.